Publication I

Laura Koponen, Martti J. Puska, and Risto M. Nieminen. 2008. Photoabsorption spectra of small fullerenes and Si-heterofullerenes. The Journal of Chemical Physics, volume 128, number 15, 154307, 7 pages.

Photoabsorption spectra of small fullerenes and Si-heterofullerenes

Laura Koponen,[a] Martti J. Puska, and Risto M. Nieminen
Department of Engineering Physics, Helsinki University of Technology, P.O. Box 1100, FIN-02015 HUT, Finland

(Received 10 January 2008; accepted 18 March 2008; published online 16 April 2008)

We study the spectral properties of two kinds of derivatives of the carbon fullerene C_{60}, small fullerenes and Si-heterofullerenes, by *ab initio* calculations. The principal method of study is the time-dependent density-functional theory in its full time-propagation form. C_{20}, C_{28}, C_{32}, C_{36}, and C_{50}, the most stable small fullerenes in the range of C_{20}–C_{50}, are found to have characteristic features in their optical absorption spectra, originating from the geometry of the molecules in question. The comparison of measured and calculated absorption spectra is found to be a useful tool in differentiating between different, almost isoenergetic ground state structure candidates of small fullerenes. Substitutionally doped fullerenes are of interest due to their enhanced chemical reactivity. It is suggested that the doping degree can be obtained by studying the absorption spectra. For example, it is observed that the spectra gradually change when doping C_{60} up to $C_{48}Si_{12}$ so that absorption in the visible and near infrared regions increases. © *2008 American Institute of Physics*. [DOI: 10.1063/1.2907742]

I. INTRODUCTION

In addition to the best known fullerene C_{60}, which was discovered in 1985 by Kroto *et al.*, there exists a variety of smaller and larger carbon fullerenes. The smallest possible fullerene is C_{20}, which consists of 12 pentagons. Due to its high curvature, the fullerene form of C_{20} is extremely reactive. However, it has been successfully synthesized in gas phase by using organic chemistry methods.[1] Besides the fullerene, the ring and bowl forms are the possible lowest-energy structure candidates for C_{20}.[2] The crossover to fullerene being systematically the most stable isomer of C_n takes place around $n=26-30$ (see, e.g., Ref. 3).

Since the early days of the fullerene studies, it has been possible to produce small fullerenes in the gas phase with a wide distribution of masses. For example, in Ref. 4, the highest intensities of the mass spectroscopy were found between C_{32}–C_{50}. C_{32} was found the most abundant species, followed by C_{36}, C_{44}, and C_{50}. Of those fullerenes, sometimes called magic ones, only C_{36} has been obtained as pure solid so far.[5] C_{28} has also attracted special interest as many endohedral metallofullerenes $M@C_{28}$ have been synthesized and characterized.[6]

The properties of fullerenes can also be modified by adding functional groups or substituting some of the carbon atoms by other elements. An interesting candidate for substitutional doping is silicon, which lies just beneath carbon in group IV of the Periodic Table of elements. Si-heterofullerenes $C_{n-m}Si_m^+$ have been produced in laser vaporization experiments in the range of $n=32-80$ up to $m\approx 9$.[7,8] Si-heterofullerenes $C_{60-m}Si_m$ are computationally shown to be stable up to about $m=20$.[9] This might be somewhat surprising taking into account that typical Si–Si bond lengths are large, of the order of 2.4 Å, compared to C–C distances of ≈1.5 Å.

Besides predicting new isomers and compositions by direct structure calculations, computational methods can be used to predict other properties of new materials in order to characterize them. In this paper, the calculation and use of optical absorption spectra in distinguishing between different compositions and isomers is addressed. Previously, the use of absorption spectra, calculated using the full time-dependent density-functional theory (TDDFT) method, has been demonstrated in Ref. 2, where ring, bowl, fullerene, and different cage isomers of C_{20} show distinguishable spectral properties. In Ref. 10, the absorption spectra of $C_{50}Cl_{10}$, the Saturn-shaped derivative of C_{50}, has been calculated using the Casida form of TDDFT.

In this paper, we calculate the optical absorption spectra of the most interesting small fullerenes and a series of Si-heterofullerenes $C_{60-m}Si_m$ up to $m=12$. To our knowledge, this is the first time when TDDFT is systematically applied to a series of small fullerenes or derivatives of fullerenes. The main tool that we use to calculate these spectra is the TDDFT in its full time-propagation form. Before that, we optimize the geometries of the studied molecules and calculate some ground state properties using the standard DFT methods. We present results for bond lengths, relative energies, and gap energies of different isomers which are in accordance with the previous studies. The spectral calculations are insensitive to small variations in bond lengths and other ground state properties. Therefore, somewhat robust ground state calculations qualify for a starting point to the TDDFT calculations.

II. METHOD OF CALCULATION

Two computer programs are used in the geometry optimization of the studied molecules. The first one is SIESTA,[11] a

[a]Electronic mail: lak@fyslab.hut.fi.

pseudopotential based DFT code. A basis set consisting of double-zeta with polarization atomic orbitals is used in these calculations. The other program is CPMD,[12] a plane-wave pseudopotential implementation of DFT.

The main tool in this study is the OCTOPUS program[13] (Version 2.0.1). It is a real-space code, which means that no basis set is used. The OCTOPUS program includes the standard DFT for the ground state and the treatment of electronic excitations by means of time-propagating the time-dependent Kohn–Sham equations in real time.

The system is excited from its initial ground state by applying an instantaneous electric field described by the potential $v(\vec{r},t)=-k_0\gamma\delta(t)$, where $\gamma=x,y,z$ denotes the polarization direction and k_0 is the amplitude of the perturbation. This corresponds to multiplying the ground state wave functions with the exponential $e^{ik_0\gamma}$. Then, the system is let to propagate over a finite period of time. The dynamical polarizability at frequency ω is

$$\alpha_\gamma(\omega) = -\frac{1}{k_0}\int d^3r\,\gamma\delta n(\vec{r},\omega), \tag{1}$$

where $\delta n(\vec{r},\omega)$ is the time Fourier transform of the deviation of electron density from the ground state density of the system. The photoabsorption cross section is obtained by averaging over the three spatial coordinates,

$$\sigma(\omega) = \frac{4\pi\omega}{c}\frac{1}{3}\,\mathrm{Im}\left(\sum_\gamma \alpha_\gamma(\omega)\right), \tag{2}$$

where c is the speed of light. For further details of the method see, for example, Ref. 14.

The Perdew–Burke–Ernzerhof[15] (PBE) exchange-correlation potential, which is one of the generalized gradient approximation (GGA) potentials, is used in most of the calculations. In some geometry optimizations, the Becke-Lee-Yang-Parr (BLYP) GGA potential[16,17] is also tested as it is known to give accurate bond lengths for carbon structures. In addition, some calculations are performed by using the local-density approximation[18] (LDA) for comparison. If not otherwise stated, PBE is applied when presenting the results in the following sections.

Although the local and semilocal exchange-correlation functionals such as PBE are known to underestimate the highest occupied molecular orbital–lowest unoccupied molecular orbital (HOMO-LUMO) gaps, they fairly correctly produce the true gaps observed in the absorption spectra. In fact, the more sophisticated functionals do not necessarily improve the results of TDDFT calculations.[19] Even the LDA results are comparable to those of the most advanced functionals. The search for good exchange-correlation functionals for TDDFT is work in progress, with few results so far. PBE is relatively simply formulated and thus easy to treat, for example, in error analysis. Therefore, we have chosen PBE and LDA appropriate for our full time-propagation TDDFT study rather than, for example, the semiempirical hybrid functionals such as B3LYB three-parameter hybrid functional.[20]

Norm-conserving Troullier–Martins pseudopotentials[21] were used throughout the calculations. In the time propagation, the time step is 0.002 $\hbar$/eV and the total number of steps is set to 15 000. The total propagation time is thus 30 $\hbar$/eV $\approx$ 20 fs.

III. GEOMETRY OPTIMIZATION OF SMALL FULLERENES

The fullerenes C_n consist of 12 pentagons and $n/2-10$ hexagons. The structure of C_{60}, as well as those of the larger fullerenes, obeys the isolated pentagon rule, which results from the high strain and resonance destabilization of adjacent pentagons. As they are not avoidable in fullerenes C_n with $n<60$, the isomer with the least adjacent pentagons is the most stable one. This is the pentagon adjacency penalty rule (PAPR).[22]

Besides the experimental data briefly presented in Sec. I, there are plenty of theoretical studies concerning the structures of the small fullerenes. Based on them, we have picked the most relevant isomers to be considered in this study as follows. The studied structures are illustrated in Fig. 1. C_{20} has only one fullerenic isomer which has the form of a dodecahedron. C_{28} has two isomers of which the one with the T_d symmetry is clearly the one lower in energy.[6] The D_3 isomer is also evidently the ground state of C_{32}.[23,24] C_{36} has two low energy isomers, those with the D_{2d} and D_{6h} symmetries, which are almost isoenergetic. According to theoretical studies, it seems that the D_{2d} isomer is the ground state structure.[24,25] The experimentally produced samples were identified by NMR spectroscopy to consist of D_{6h} isomers.[5] For C_{50}, the isomers with the D_3 and the D_{5h} symmetries have the lowest energies. It is somewhat unclear as to which one of them is the ground state. For example, the calculation in Ref. 26 suggest it to be D_3, even though it does not follow PAPR.

Due to the Jahn–Teller distortion, the fullerenic C_{20} does not preserve its perfect I_h symmetry. There exist five almost isoenergetic candidates for the Jahn–Teller distorted lowest-energy structure.[27] We have observed that the effect of the structure deformation on the absorption spectrum is very small. Therefore, in this paper, we consider mainly the symmetric I_h structure. C_{28}, the other studied molecule with an open-shell ground state, did not show a Jahn–Teller distortion.[24]

It is noteworthy that the ground state structure may also depend on the charge of the molecule. For example, the ground state structure of the charged C_{20}^{2+} does have the perfect I_h symmetry and for C_{50}^{+}, C_{50}^{-}, and C_{50}^{2-}, the D_{5h} isomer is calculated to be clearly lower in energy than the D_3 structure.[28] In gas-phase experiments, the particles are usually C_n^- anions.

The bond lengths of the small fullerenes are calculated with the SIESTA code, using both the PBE and LDA functionals. The resulting bond lengths are shown in Table I. The shapes of the molecules and the bond lengths agree well with the previously published results.[29]

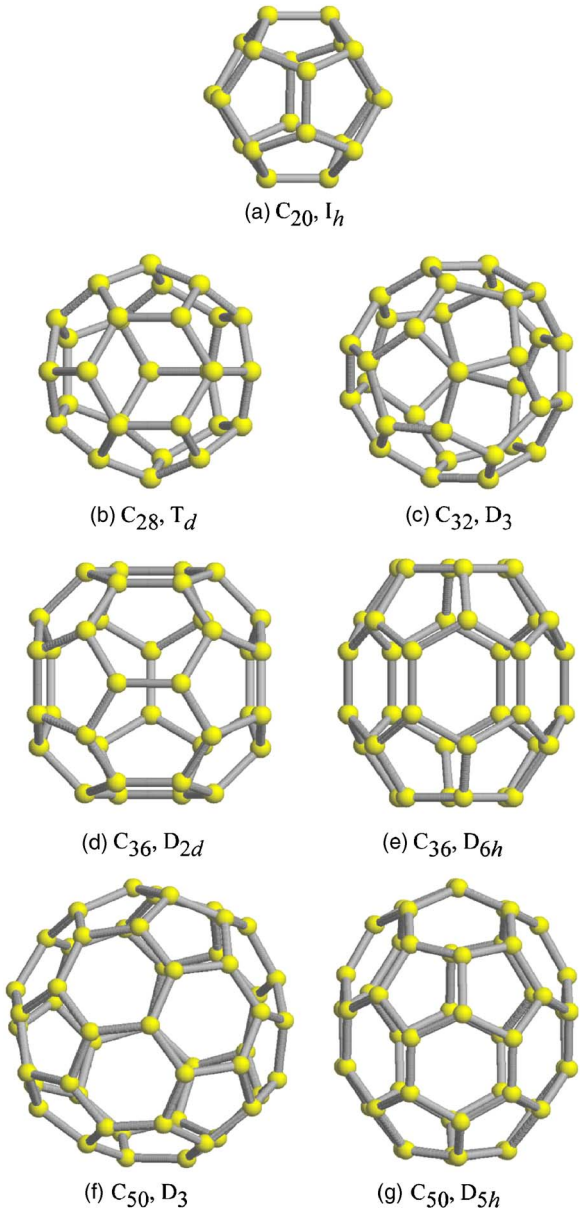

FIG. 1. (Color online) Structures of the studied small carbon fullerenes.

IV. GEOMETRY OPTIMIZATION OF Si-DOPED FULLERENES

The structures of several heterofullerenes in the range of $C_{60}-C_{48}S_{12}$ have been calculated previously by using SIESTA within the LDA approximation in Ref. 30. Based on these results, completed with those of Ref. 31 for $C_{54}Si_6$, a representative set of low-energy structures was selected in this study. In summary, the silicon atoms in $C_{60-m}Si_m$ tend to sit next to each other for $m>2$. For $m=2$, there are several low-energy isomers with different Si–Si distances.

The studied structures are shown in Fig. 2. The labeling of different isomers of $C_{58}Si_2$ and $C_{54}Si_6$ follows Refs. 30 and 31, respectively. For the isomers of $C_{58}Si_2$, the label number increases as the distance between the two silicon atoms grows.

The geometry optimization of Si-heterofullerenes is done by using both SIESTA (PBE potential) and CPMD (BLYP potential) independently. The results are very similar. As we pointed out in Sec. I, due to the insensitivity of the TDDFT calculations to small variations of the structure, the geometries produced by the two methods can be deduced to be identical starting points for the TDDFT calculation. The bond lengths of the structures obtained from the CPMD calculations are tabulated in Table II. The results are in good accordance with those of Refs. 30 and 31. Note that in Ref. 30, the LDA potential is used, which clearly underestimates the bond lengths compared to the more accurate PBE or BLYP.

TABLE I. Bond lengths of the studied molecules. All bond lengths are given in Å. hh, hp, and pp stand for hexagon-hexagon, hexagon-pentagon, and pentagon-pentagon bonds. No. indicates the number of bonds of each type.

Species and isomer	PBE	LDA	No.
C_{20}, I_h	1.469 pp	1.455 pp	30
C_{28}, T_d	1.449 hp	1.436 hp	24
	1.46–1.52 pp	1.45–1.51 pp	18
C_{32}, D_3	1.470 hh	1.455 hh	3
	1.40–1.48 hp	1.39–1.47 hp	30
	1.46–1.51 pp	1.44–1.50 pp	15
C_{36}, D_{2d}	1.46–1.47 hh	1.44–1.45 hh	6
	1.41–1.47 hp	1.40–1.46 hp	36
	1.49 pp	1.47–1.48 pp	12
D_{6h}	1.458 hh	1.444 hh	6
	1.43–1.45 hp	1.42–1.44 hp	36
	1.502 pp	1.487 pp	12
C_{50}, D_3	1.41–1.46 hh	1.40–1.45 hh	21
	1.44–1.49 hp	1.43–1.47 hp	48
	1.461 pp	1.447 pp	6
D_{5h}	1.42–1.43 hh	1.40–1.42 hh	20
	1.44–1.48 hp	1.42–1.46 hp	50
	1.478 pp	1.469 pp	5
C_{60}, I_h	1.418 hh	1.406 hh	30
	1.468 hp	1.453 hp	60

V. RESULTS FOR SMALL FULLERENES

Table III shows the ground state properties of the studied molecules. As expected, the binding energy per atom increases steadily when the size of the fullerene decreases. C_{32}, the isomer D_{5h} of C_{50} and C_{60}, have the largest HOMO-LUMO gaps of 1.25–1.55 eV, while the other studied structures have gaps close to zero or zero (degenerate partly filled HOMO).

The photoabsorption spectra of the studied small fullerenes are shown in Figs. 3–5. All of the spectra have a similar general composition. There is an empty gap area at the lowest energies, some minor peaks at about 1–4 eV and one or several main peaks between 4 and 7 eV which originate from π-π^* transitions. Then, some more peaks follow at 7–12 eV, continuing as a broad feature up to about 50 eV (see inset in Fig. 7). The energy range far beyond the ionization energy of about 7–8 eV is of little interest since the TDDFT method does not handle it correctly and it is also experimentally harder to access.

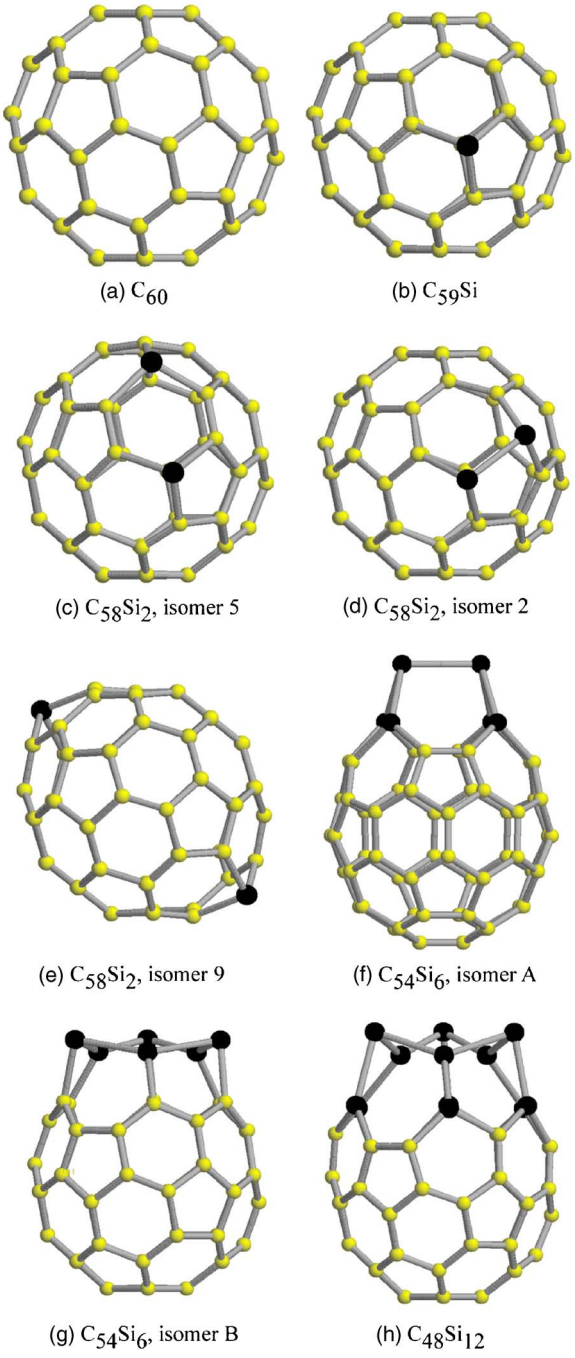

FIG. 2. (Color online) Structures of the studied Si-doped carbon fullerenes.

Figure 6 shows that the energy of the main peak of the spectrum, corresponding to a collective mode of π-electrons, gradually increases from about 4.7 to 5.8 eV, as the size of the fullerene increases from C_{20} to C_{60}. The increase is not expected to be exactly linear since the energy of the collective excitation depends on the specific geometry of each molecule. Especially, the D_{6h} symmetric isomer of C_{36} differs from the trend due to its highly nonspherical shape. Still, the energy of the main peak is an important measure which is mainly determined by the size of the fullerenes.

The Jahn–Teller distortion is found to have only a minor effect on the absorption spectra of C_{20}. This is illustrated in Fig. 3, where the spectra of the undistorted structure and the D_{3d} symmetric distorted structure are shown. The overall shapes coincide to a high degree, but the distorted structure has a slightly wider main peak at 4.75 eV and it is shifted by 0.1 eV toward higher energies, as are also the peaks at 7–12 eV. These differences reflect the slightly stronger bonds and larger scatter in the bond strengths in the distorted case. However, the differences are minor, and thus, the accuracy of the method does not allow it to be considered useful in experimental characterization of the different Jahn–Teller distorted structures.

Below the main excitation peak, C_{20} has a single peak at 3.6 eV. The spectrum has also a characteristic, almost empty region at 4.9–6.7 eV. C_{28} and C_{32} have fairly similar absorption spectra, with little intensity below the main peak and several peaks in the range of 6–12 eV, especially at 8–9 and 10–11 eV. The two studied isomers of C_{36} are easy to distinguish. The absorption spectrum of the D_{2d} isomer is dominated by the main excitation at 5.3 eV. On the contrary, the main excitation of the D_{6h} isomer is split into two adjacent peaks at 5.2 and 5.6 eV. The reason lies in the elongated structure of the isomer. The lower peak originates from the collective excitation along the long axis of the molecule and the upper one from the excitations along the plane perpendicular to it. The absorption spectra of the two isomers of C_{50} also have clear characteristics. The D_{5h} isomer has sharp

TABLE II. Bond lengths of the studied molecules. All bond lengths are given in Å. hh, hp, and pp stand for hexagon-hexagon, hexagon-pentagon, and pentagon-pentagon bonds.

Species and isomer	C–C	C–Si	Si–Si
$C_{59}Si$	1.40–1.43 hh	1.848 hh	···
	1.46–1.51 hp	1.900 hp	···
$C_{58}Si_2$, 5	1.40–1.45 hh	1.862 hh	···
	1.47–1.50 hp	1.88–1.92 hp	···
$C_{58}Si_2$, 2	1.40–1.44 hh	1.847 hh	2.303 hp
	1.46–1.50 hp	1.916 hp	···
$C_{58}Si_2$, 9	1.40–1.43 hh	1.848 hh	···
	1.46–1.51 hp	1.900 hp	···
$C_{54}Si_6$, A	1.40–1.43 hh	1.872 hh	2.661 hh
	1.45–1.50 hp	1.928 hp	2.411 hp
$C_{54}Si_6$, B	1.41–1.42 hh	1.90–1.98 hp	2.360 hh
	1.46–1.53 hp		2.372 hp
$C_{48}Si_{12}$	1.41–1.44 hh	1.83–1.85 hh	2.425 hh
	1.46–1.48 hp	1.82–1.84 hp	2.32–2.48 hp

TABLE III. HOMO-LUMO gaps and binding energies per atom. The latter are given with respect to C_{60}. The values are calculated by using the OCTOPUS program.

Species	Gap	ΔE/atom
C_{20} (I_h)	0	0.90
C_{20} (D_{3d})	0.56	0.85
C_{28} (T_d)	0	0.6
C_{32} (D_3)	1.40	0.37
C_{36} (D_{2d})	0.40	0.27
C_{36} (D_{6h})	0.45	0.34
C_{50} (D_3)	1.25	0.10
C_{50} (D_{5h})	0.26	0.12
C_{60} (I_h)	1.55	0

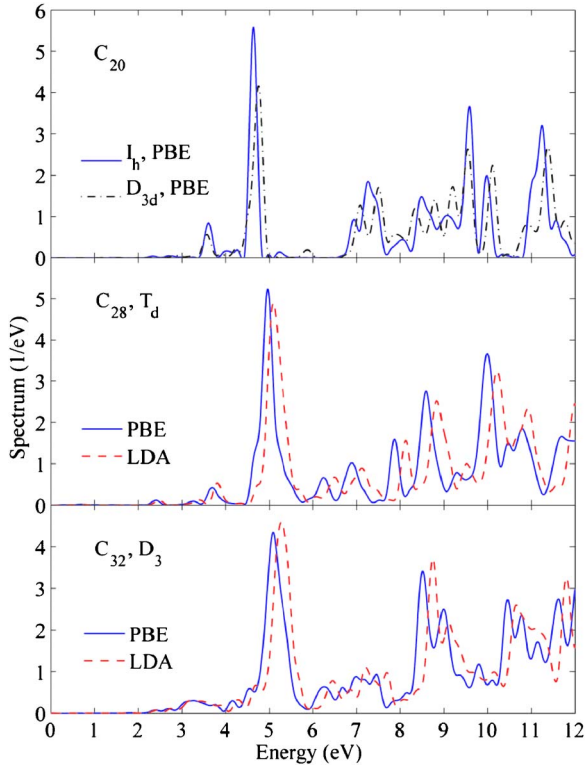

FIG. 3. (Color online) Calculated photoabsorption spectra of C_{20} (symmetric and Jahn–Teller distorted structure), C_{28}, and C_{32}.

peaks at 3.2, 5.4, and 6.0 eV, whereas the spectrum of the D_3 isomer has a smoother spectrum. It is composed of a larger number of separate lower intensity peaks in the range of 4–6.5 eV; the adjacent ones of which are partly fused together. This reflects the lower degeneracy of the electron states in the D_3 symmetry. The main characteristic excitations occur at 5.4 V and 6.2 eV which coincide with those of the D_{5h} isomer, but the distinction can be drawn by the lower energy peaks. The D_3 isomer has a series of small peaks at energies of 2–4 eV, the clearest of which occurs at 2.5 eV.

Contrary to static DFT calculations, it is still generally unclear whether the PBE or other existing sophisticated functionals improve the results in TDDFT compared to the LDA. In this study, the LDA and PBE functionals give very similar absorption spectra except that the LDA spectra are systematically about 3% higher in energy than PBE spectra. This corresponds to a 0.15 eV shift in 5 eV energy. The shift is mainly caused by the stronger bonds of the LDA calculations, which directly increases the absorption frequencies.

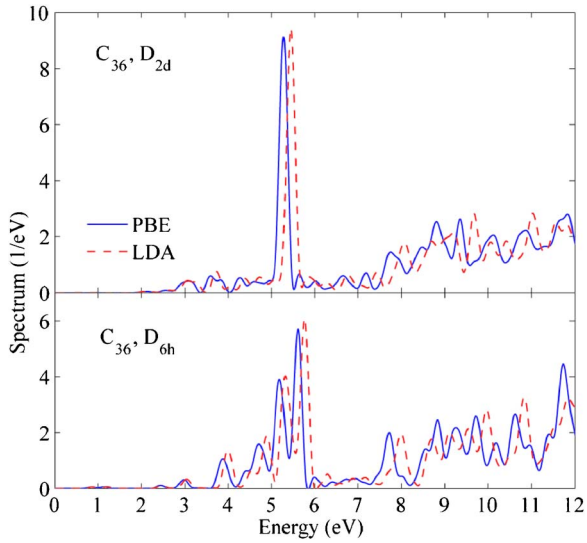

FIG. 4. (Color online) Calculated photoabsorption spectra of the two studied isomers of C_{36}.

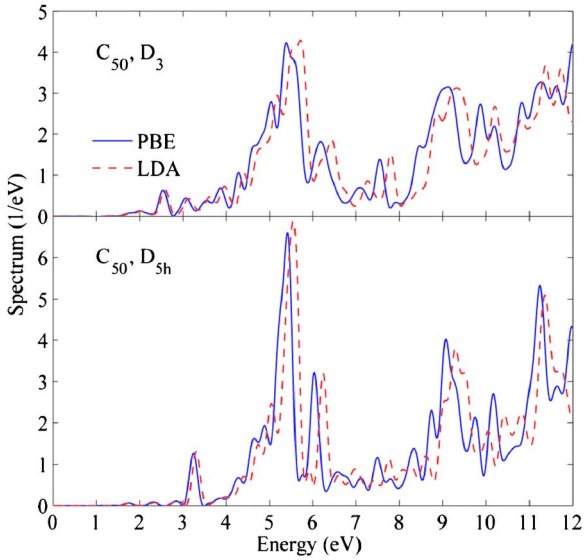

FIG. 5. (Color online) Calculated photoabsorption spectra of the two studied isomers of C_{50}.

VI. RESULTS FOR Si-DOPED FULLERENES

The HOMO-LUMO gaps and the relative total energies of different isomers, obtained from ground state calculations, are presented in Table IV. The relative total energies of the three studied isomers of $C_{58}Si_2$ follow the previously published results,[30] whereas the relative total energies of the two isomers of $C_{54}Si_6$ do not agree with Ref. 31. As our main focus is not the ground state properties, we leave any further investigation of the matter.

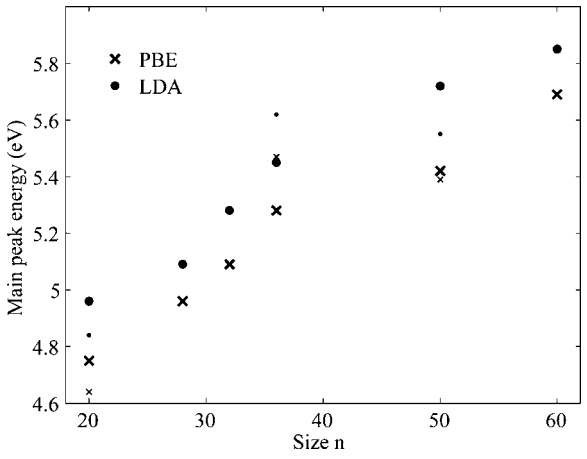

FIG. 6. Energy of the main peak in the absorption spectrum of the studied small fullerenes in the range C_{20}–C_{60}. The smaller marks represent isomers with slightly higher energy in cases where two isomers are studied, that is, I_h isomer of C_{20}, D_{6h} isomer of C_{36}, and D_{5h} isomer of C_{50}.

TABLE IV. HOMO-LUMO gaps and relative total energies of different isomers compared to the ground state isomer energy. Our results are calculated by using the OCTOPUS program.

Species	Gap	ΔE		Ref.
$C_{59}Si$	1.10	⋯		⋯
$C_{58}Si_2$, 5	0.62	0	0	30
$C_{58}Si_2$, 2	0.84	0.33	0.21	30
$C_{58}Si_2$, 9	1.03	0.52	0.66	30
$C_{54}Si_6$, A	0.92	1.41	0	31
$C_{54}Si_6$, B	0.96	0	0.05	31
$C_{48}Si_{12}$	0.37	⋯		⋯

The series of absorption spectra from C_{60} to $C_{48}Si_{12}$ are presented in Figs. 7–9. The spectrum of C_{60} is composed of a wide empty region up to about 2.5 eV, a series of four clear peaks of increasing intensity at 3–6 eV, and some broader peaks above it. Substituting one carbon atom with silicon shrinks the gap and induces a series of low-intensity peaks in the range of 1–3 eV. The features of the spectrum are also smeared due to the symmetry break and the variations in the C–C bond strengths.

The three isomers of $C_{58}Si_2$ have some small but characteristic differences in their absorption spectra, especially in the visible region. At the energy range of 2–4 eV, all those isomers have three clear excitations but their energies vary. Isomer 9 has lowest and the highest of those peaks at 2.1 and 4.3 eV, whereas isomer 2 shows them at 2.5 and 4.0 eV, respectively. Isomer 5 has the middle peak at 3.5 eV, whereas isomers 9 and 2 have it at 3.2 eV.

One could expect a strong resemblance between the absorption spectra of $C_{59}Si$ and the isomer 9 of $C_{58}Si_2$, where the two silicon atoms are situated on the opposite sides of the fullerene. However, this is not observed. Thus, the mutual interplay between the silicon atoms is not suppressed when their distance is increased.

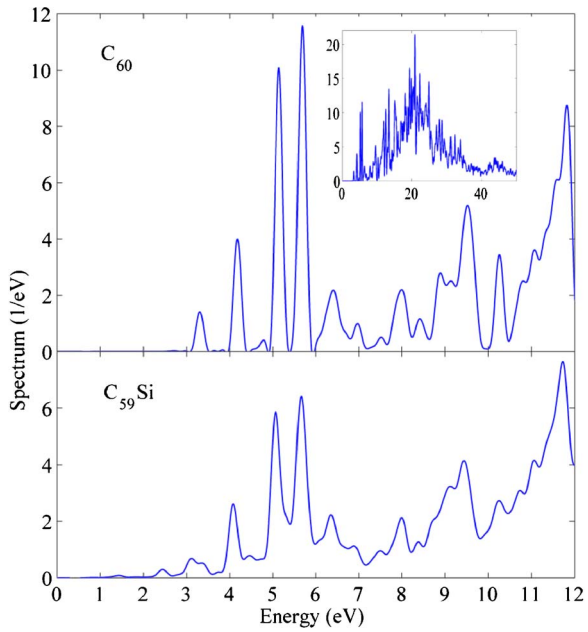

FIG. 7. (Color online) Calculated photoabsorption spectra of C_{60} and $C_{59}Si$. The spectrum of C_{60} up to 50 eV is shown in the inset.

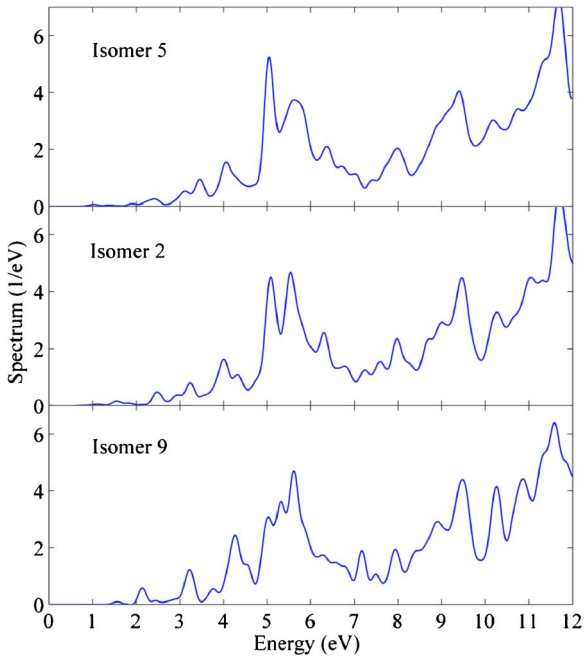

FIG. 8. (Color online) Calculated photoabsorption spectra of three low-energy isomers of $C_{58}Si_2$.

Isomers A and B of $C_{54}Si_6$ have similar absorption spectra and the differences between them are so small that no reliable distinction can be made between them. $C_{48}Si_{12}$ has a smeared absorption spectrum that extends from 0.6 eV up to energies beyond the ionization potential.

Figure 10 shows an example of the HOMO and LUMO

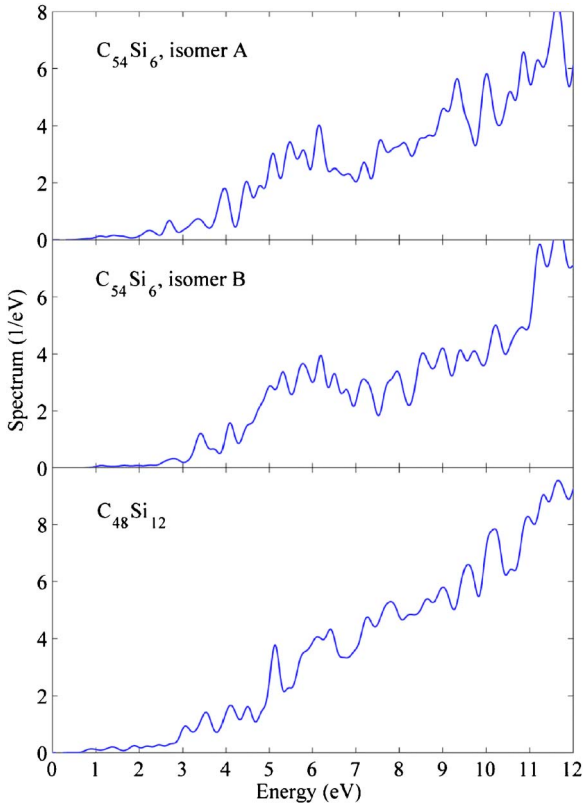

FIG. 9. (Color online) Calculated photoabsorption spectra of two low-energy isomers of $C_{54}Si_6$ and $C_{48}Si_{12}$.

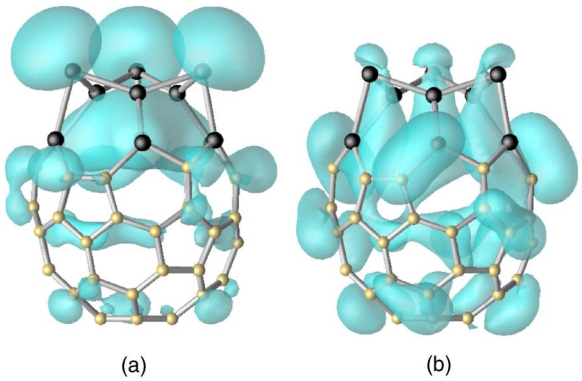

FIG. 10. (Color online) HOMO and LUMO states of $C_{48}Si_{12}$ (shown only the positive part of the wave functions for clarity).

orbitals for $C_{48}Si_{12}$. In all Si-heterofullerenes, the HOMO and LUMO orbitals are mainly localized on the Si atoms, as in Fig. 10(a) or, in some cases, also on the C atoms bonded to Si atoms, as in Fig. 10(b). Our observations agree with those of Ref. 32, where the localization issues of $C_{59}Si$ and $C_{58}Si_2$ have been discussed in detail.

VII. CONCLUSIONS

We have calculated the optical absorption spectra of a series of small fullerenes and Si-doped buckminsterfullerenes. The studied small fullerenes show a trend of an increasing energy of the main excitation from 4.7 to 5.8 eV as the size of the molecule increases from C_{20} to C_{60}. The two ground state candidate isomers of C_{36} and C_{50} show distinctive features in their spectra. Thus, the computational results could be used in determining the isomer structures of samples in experiments.

Substitutional doping of C_{60} with silicon induces new absorption peaks into the spectrum, especially introducing some absorption strength in the visible range and near infrared range. For structures with just a few Si dopant atoms, the absorption spectra show composition-and isomer-dependent features. For example, the three studied low-energy isomers of $C_{58}Si_2$ can be distinguished by our spectrum calculations. As the number of the dopant atoms is increased to 6 and further to 12, the peaks form smeared broad features and no fingerprints of specific molecules and isomers can be seen.

The systematic full time-propagation TDDFT study of medium-sized molecules such as fullerenes is currently in the limits of existing computational capabilities. Due to the favorable scaling O(N) of the TDDFT method with respect to the electron number *N*, its applications to larger systems are expected in future as the computational resources develop. The full time-propagation method is competent for treating the excitations in clusters and molecules such as fullerenes, but it is currently not successfully applicable to many other systems involving phenomena such as excitonic behavior or charge transport. Theoretical research in order to widen the applicability of TDDFT is continuously going on in the field.

ACKNOWLEDGMENTS

This research is supported by the Academy of Finland through the Centers of Excellence Program (2006-2011). CSC, the Finnish IT center for science, is acknowledged for providing computer resources. We thank Dr. Masahiko Matsubara for assistance in geometry optimization.

[1] H. Prinzbach, A. Weiler, P. Landenberger, F. Wahl, J. Wörth, L. T. Scott, M. Gelmont, D. Olevano, and B. v. Issendorff, Nature (London) **407**, 60 (2000).
[2] A. Castro, M. A. L. Marques, J. A. Alonso, G. F. Bertsch, K. Yabana, and A. Rubio, J. Chem. Phys. **116**, 1930 (2002).
[3] P. R. C. Kent, M. D. Towler, R. J. Needs, and G. Rajagopal, Phys. Rev. B **62**, 15394 (2000).
[4] H. H. Kietzmann, R. Rochow, G. Ganteför, W. Eberhardt, K. Vietze, G. Seifert, and P. W. Fowler, Phys. Rev. Lett. **81**, 5378 (1998).
[5] C. C. Piskoti, J. Yarger, and A. Zeitl, Nature (London) **393**, 771 (1998).
[6] X. Lu and Z. Chen, Chem. Rev. (Washington, D.C.) **105**, 3643 (2005).
[7] C. Pellarin, M. Ray, J. Lermé, J. L. Vialle, M. Broyer, X. Blase, P. Kéghélian, P. Mélinon, and A. Perez, J. Chem. Phys. **110**, 6927 (1999).
[8] X. Blase, M. Broyer, P. Kéghélian, J. Lermé, P. Mélinon, M. Pellarin, A. Perez, C. Ray, and J. L. Vialle, Eur. Phys. J. D **9**, 49 (1999).
[9] M. Matsubara, J. Kortus, J.-C. Parlebas, and C. Massobrio, Phys. Rev. Lett. **96**, 155502 (2006).
[10] R.-H. Xie, G. W. Bryan, C. F. Cheung, V. H. J. Smith, and J. Zhao, J. Chem. Phys. **121**, 2849 (2004).
[11] J. M. Soler, E. Artacho, J. D. Gale, A. García, J. Junquera, P. Ordejón, and D. Sánchez-Portal, J. Phys.: Condens. Matter **14**, 2745 (2002); See: http://www.uam.es/departamentos/ciencias/fismateriac/siesta/.
[12] CPMD, Copyright IBM Corp 1990–2006, Copyright MPI für Festkörperforschung Stuttgart, 1997–2001 (http://www.cpmd.org).
[13] A. Castro, H. Appel, M. Oliveira, C. A. Rozzi, X. Andrade, F. Lorenzen, M. A. L. Marques, E. K. U. Gross, and A. Rubio, Phys. Status Solidi B **243**, 2465 (2006); See: http://www.tddft.org/programs/octopus/.
[14] *Time-Dependent Density Functional Theory*, edited by M. A. L. Marques, C. A. Ullrich, F. Nogueira, A. Rubio, K. Burke, and E. K. U. Gross (Springer-Verlag, Berlin, 2006).
[15] J. P. Perdew, K. Burke, and M. Ernzerhof, Phys. Rev. Lett. **77**, 3865 (1996).
[16] A. D. Becke, Phys. Rev. A **38**, 3098 (1988).
[17] C. Lee, W. Yang, and R. G. Parr, Phys. Rev. B **37**, 785 (1988).
[18] J. P. Perdew and A. Zunger, Phys. Rev. B **23**, 5048 (1981).
[19] M. A. L. Marques, A. Castro, and A. Rubio, J. Chem. Phys. **115**, 3006 (2001).
[20] P. J. Stephens, F. J. Devlin, C. F. Chabalowski, and M. J. Frisch, J. Phys. Chem. **98**, 11623 (1994).
[21] N. Troullier and J. L. Martins, Phys. Rev. B **43**, 1993 (1991).
[22] E. E. B. Campbell, P. Fowler, D. Mitchell, and F. Zerbetto, Chem. Phys. Lett. **250**, 544 (1996).
[23] Y. Chang, A. F. Jalbout, J. Zhang, Z. Su, and R. Wang, Chem. Phys. Lett. **428**, 148 (2006).
[24] B. Paulus, Phys. Chem. Chem. Phys. **5**, 3364 (2003).
[25] G. Zheng, S. Irle, and K. Morokuma, Chem. Phys. Lett. **412**, 210 (2005).
[26] W. Q. Tian, J.-K. Feng, Y. A. Wang, and Y. Aoki, J. Chem. Phys. **125**, 094105 (2006).
[27] Z. Chen, T. Heine, H. Jiao, A. Hirsch, W. Thiel, and P. v. R. Schleyer, Chem.-Eur. J. **10**, 963 (2004).
[28] S. Díaz-Tendero, M. Alcamí, and F. Martín, Chem. Phys. Lett. **407**, 153 (2005).
[29] E. Malolepsza, H. A. Witek, and S. Irle, J. Phys. Chem. A **111**, 6649 (2007).
[30] C.-C. Fu, M. Weissman, M. Machado, and P. Ordejón, Phys. Rev. B **63**, 085411 (2001).
[31] M. Matsubara and C. Massobrio, J. Chem. Phys. **122**, 084304 (2005).
[32] C. Billas, I. M. L. Massobrio, M. Boero, M. Parrinello, W. Branz, F. Tast, N. Malinowski, M. Heinebrodt, and T. P. Martin, J. Chem. Phys. **111**, 6787 (1999).